International Research Journal of Natural and Applied Sciences
ISSN: (2349-4077)
Impact Factor 7.032 Volume 9, Issue 07, July 2022
Website- www.aarf.asia, Email : editor@aarf.asia , editoraarf@gmail.com

Geometry Dependent Interference Effects in Coupled Triple Quantum Dots

Gagan Rajput

Department of Physics, Vallabh Government College, Mandi-175001 India

Abstract

Electronic transport through a coupled triple quantum dot (TQD) system in T-shape and triangular shape configuration is theoretically studied using Keldysh's non-equilibrium Green's function approach. It is observed that in the T-shape configuration, an antiresonance peak appears in the electronic transport spectrum at the quantum dot (QD) energy level which results from the quantum interference effects that take place in electron transport through multiple channels. The width of the antiresonance peak increases with the increase in interdot tunnel coupling in the side coupled QD. Further, an asymmetric Fano lineshape is found to occur in the triangular shape configuration for a particular case when side coupled QD is symmetrically coupled to other two QDs which are connected to leads in a series configuration. This asymmetric Fano lineshape can be attributed to the destructive quantum interference effect taking place in the electron transport through multiple pathways.

Keywords: Coupled Triple Quantum Dots, T-Shape and Triangular Shape configurations; Interference Effects; Fano Effect.

1. Introduction

Quantum dots (QD)s have been studied in the recent past by various authors[1-17] due to their rich potential applications. Electron transport through the QD systems has been utilized to study various physical phenomena such as interference effects, Kondo effect, dephasing effect, quantum entanglement, swap effect, and Coulomb blockade in low dimensional systems [1-4, 6-17]. A distinct feature of electronic transport through the QD systems is quantum phase coherence which is manifested through interference effects in various QD structures. Therefore, various structures of multiply connected QDs i.e. two, three, four and an array of a finite number of QDs have been studied in the last few years.

The TQD systems have been investigated [14-17] particularly for their use in spin qubits, charge qubits, charging rectifiers, and in the study of correlation effects. The interference effect in terms of the Fano effect and formation of bound states in the continuum (BIC) due to magnetic flux in TQD systems has already been studied, but, structural dependent interference effects in these systems have not been discussed so far to the best of knowledge. Therefore, the electronic transport through the TQD system is studied, here, in T-shape and triangular shape configurations to investigate interference effects. In a T-shape configuration, the QDs, QD1 & QD2 are connected to the left and right lead respectively and coupled to each other with the interdot tunnel couplingt_{12}, whereas QD3 is side coupled to QD2 with tunnel coupling t_{23}. Triangular shape configuration is obtained when QD3 is also coupled to QD1 with the interdict tunnel couplingt_{13}. Response of the system for the transition from the T-shape to the triangular shape configuration is examined by varying t_{13}.

Using Keldysh non-equilibrium Green's function approach [18] for three impurities Anderson Hamiltonian [19], various Green's functions are derived in the Coulomb blockade (CB) regime with the help of equations of motion and decoupling scheme as used in Ref. [20]. In the electronic transport spectrum for T-shape configuration, $t_{23} \neq 0$, an antiresonance peak is found to occur at QD's energy level. The width of this peak increases with the increase in the value of interdot tunnel coupling t_{23}. This behavior of the TQD system in a T-shape configuration can be understood in terms of the quantum interference effect that takes place between discrete states and the continuum in transport through different pathways.

Further, it is also found that when QD geometry is transitionally changed from the T-shape tote triangular shape configuration, asymmetric Fano lineshape occurs for the triangular shape configuration for a symmetrical coupling of side coupled QD, QD3, with other two QDs, QD1 & QD2, which are serially coupled to each other. The asymmetric Fano lineshape can be attributed to the destructive quantum interference effect that takes place between discrete states and the continuum in electronic transport. Thus, quantum interference effects, as revealed in terms of the antiresonance peak and the asymmetric Fano lineshape in the electron transport through different QD structures, can be tuned with various interdot tunnel couplings. Main focus in this work is to study the interference effects, so, interaction effects are not considered here.

The paper is organized in six sections: in section 2 mathematical formulations is done. Results are discussed in section 3. Conclusions are given in section 4 whereas Appendices A and B are given in section 5 and section 6 respectively.

2. Mathematical Formulation

A coupled TQD system is described by three impurities Anderson Hamiltonian [19] as;

$H = H_l + H_d + H_t$, (1)

where, l, d, and t in the above equation reads as leads, dots, and tunnel respectively, and

$H_l = \sum_{k\alpha\sigma} \epsilon_k^\alpha c_{k\alpha\sigma}^\dagger c_{k\alpha\sigma}$,

$H_d = \sum_{i\sigma} \epsilon_i d_{i\sigma}^\dagger d_{i\sigma} + \sum_i U_i n_{i\sigma} n_{i-\sigma}$,

$H_t = \sum_\sigma (t_{12} d_{1\sigma}^\dagger d_{2\sigma} + t_{23} d_{2\sigma}^\dagger d_{3\sigma} + t_{13} d_{1\sigma}^\dagger d_{3\sigma} + h.c. + \sum_{ik\alpha\sigma} V_{ik}^\alpha c_{k\alpha\sigma}^\dagger d_{i\sigma} + h.c.)$ (2)

Where $c_{k\alpha\sigma}^\dagger$ ($c_{k\alpha\sigma}$) is the creation (annihilation) operator in the lead with ϵ_k^α as the energy of the lead. The left/right (L/R) lead is represented by α = L(R) and spin by σ. Similarly, the creation (annihilation) operator of the QDs is represented by $d_{i\sigma}^\dagger (d_{i\sigma})$ with i=1, 2, 3. The single electron energy level, intradot Coulomb interaction energy, and hybridization between the QDs and the leads are represented by ϵ_i, U_i, and V_{ik}^α respectively. The interdot tunnel couplings are represented by t_{12}, t_{23}, and t_{13}. A mathematical formulation has been derived for the coupled TQD system using Keldysh non-equilibrium Green's function formalism [18]. Using the equation of motion and proper decoupling schemes [20] various (retarded, advanced, and lesser) Green's functions are derived in Coulomb Blockade (CB) regime. The current in the steady state condition is derived from the formula [20],

$$I_e = \frac{2e}{h} \int [f_L(\omega) - f_R(\omega)] T(\omega) d\omega. \quad (3)$$

In the above equation, $f_\alpha(\omega) = [1 + e^{(\omega - \mu_\alpha)/K_B T}]^{-1}$ represents the Fermi distribution function in leads with chemical potential μ_α. The transmission coefficient, T (ω), is derived from the formula,

$T(\omega) = \mathbf{tr\{ G^a \Gamma^R G^r \Gamma^L \}}$ (4)

where,

$\Gamma^\alpha = (\Gamma_{11}^\alpha \Gamma_{12}^\alpha \Gamma_{13}^\alpha \Gamma_{21}^\alpha \Gamma_{22}^\alpha \Gamma_{23}^\alpha \Gamma_{31}^\alpha \Gamma_{32}^\alpha \Gamma_{33}^\alpha)$ and $G^\beta = \left(G_{11}^\beta G_{12}^\beta G_{13}^\beta G_{21}^\beta G_{22}^\beta G_{23}^\beta G_{31}^\beta G_{32}^\beta G_{33}^\beta\right)$ where α=L(R) and β= r/a i.e. retarded/ advanced Greens functions. Γ^α 's, a measure of dot-lead coupling strength are defined as $\Gamma_{ij}^\alpha = 2\pi \sum_k V_{ik}^\alpha V_{jk}^{\alpha\dagger} \delta(\omega - \epsilon_k^\alpha)$. The expressions for these Green's functions in the above equation are given in Appendix A. Substituting for these Greens's functions in Eqn. (4) and solving the trace, the transmission coefficient so obtained is utilized in the next section for the discussion.

3. Results and Discussion

All the parameters in numerical calculations are scaled in terms of Γ. In this work, interaction effects are relaxed, so, intradot Coulomb interactions are taken zero as $U_1 = U_2 = U_3 = 0$ and QDs energy level values are taken $\epsilon_1 = \epsilon_2 = \epsilon_3 = \epsilon = -2\Gamma$. Results are discussed for T-shape and triangular shape geometries of TQD system which can be obtained by taking various Γ_{ii}'s, Fig. 1, as $\Gamma_{11}^{L} = \Gamma_{22}^{R} = \Gamma$and $\Gamma_{22}^{L} = \Gamma_{33}^{L} = \Gamma_{11}^{R} = \Gamma_{33}^{R} = 0$. In T-shape configuration, the interdot tunnel couplings t_{12} and t_{23} can vary while t_{13} is fixed zero and in a triangular shape configuration, all the three interdot tunnel couplings can vary. The transition from the T-shape to the triangular shape can also be investigated in this case.

Here, the transmission coefficient, T(ω), is calculated as a function of electron energy, ω. The numerical calculation is presented in two parts. In the first part, we study the T-shape configuration of the TQD system, and calculations are done for fixed values of t_{12} and $t_{13} = 0$ while varying t_{23}. In the second part, the behavior of coupled TQD system is examined for triangular shape configuration with fixed values of t_{12} and t_{23} while varying t_{13}.

Fig. 2 displays the transmission coefficient, T(ω), as a function of electron energy, ω, for the T-shape configuration of the TQD system. The interdot tunnel coupling between QD1 & QD2 is fixed as t_{12} = Γ and between QD2 & QD3, t_{23} is varied in steps to see its effect on electronic transport. Starting with t_{23}=0, a case of serially coupled double quantum dots, a pair of resonant peaks occur around QD energy level $\epsilon = -2\Gamma$. With the introduction of t_{23}, the T-shape structure starts to build up and an antiresonance peak occurs at $\epsilon = -2\Gamma$. The width of the antiresonance peak increases with an increase in t_{23}. The occurrence of the antiresonant peak can be linked with destructive quantum interference taking place through different pathways of discrete molecular states and the continuum in electron transport in the QDs.

In Fig. 3, transitional change in configuration from T-shape to triangular shape is examined for electron transport in TQD system. Here, the values of interdot couplings are taken as t_{12} = Γ, t_{23}= Γ/4 while t_{13} is varied. For t_{13} = 0 i.e. T-shape configuration, the electronic transport spectrum shows an antiresonance peak at QD's energy level as discussed above in Fig. 2. When we take t_{13} = Γ/4, a case that represents a symmetrical coupling of the side coupled QD, i.e. QD3 with QD1 & QD2, an asymmetric Fano lineshape occurs in the vicinity of QD's energy level. The occurrence of the Fano lineshape corresponds to the destructive quantum interference as discussed above. However, with a further the increase in

the value of $t_{13,}$ the Fano lineshape disappears and a small bump that takes a shape of a plateau develops towards the right side of QD's energy level, $\epsilon = -2\Gamma$. Therefore, it can be inferred from this discussion that quantum interference effects occur in both the geometries of TQD but the Fano effect, in particular, occurs only in the triangular shape configuration of the TQD system even that for the symmetrical coupling of the side coupled QD , QD3, with the serially coupled QDs, QD1 & QD2.

Therefore, the interference effect, in the form of the antiresonance peak and the asymmetric Fano lineshape, can be tuned with interdot tunnel coupling in the TQD system for different geometries.

4. Conclusions

The electronic transport property of the TQD system has been studied using three impurities Anderson Hamiltonian and Keldysh's non-equilibrium Green's function formalism. This work focuses mainly on the geometrically tunable interference effects in the TQD system, so, interaction effects are not taken up here.

Though it is now clear that the interference effects in general occur in both the geometries of the TQD system, i.e. a T-shape and triangular shape, however, its effect is different. The interference effect in T-shape configuration forms antiresonance peak in electronic transport spectrum, whereas asymmetric Fano lineshape is formed in triangular shape geometry and that even for a symmetrical coupling of side coupled QD. Both these effects are caused by the destructive quantum interference effect that takes place between discrete (molecular) states and the continuum in electron transport through different channels provided by the TQD system in these geometries. However, the difference lies in the fact that the molecular states in triangular shape TQD geometry have a long lifetime which forms asymmetric Fano lineshape in a particular case. Thus, tunable interdot tunnel couplings, which are varied to produce different TQD geometries, are found responsible for the occurrence of interference effects in these systems.

5. Appendix A

Expressions for various retarded functions are as below,

$$G_{11}^r = \frac{1}{|Z|}[P_{23} + \imath Q_{23}], G_{21}^r = \frac{1}{|Z|}[R_{12} + \imath S_{12}], G_{31}^r = \frac{1}{|Z|}[R_{13} + \imath S_{13}],$$

$$G_{12}^r = \frac{1}{|Z|}[R_{12} + \imath S_{12}], G_{22}^r = \frac{1}{|Z|}[P_{13} + \imath Q_{13}], G_{32}^r = \frac{1}{|Z|}[R_{23} + \imath S_{23}],$$

$$G_{13}^r = \frac{1}{|Z|}[R_{13} + \imath S_{13}], G_{23}^r = \frac{1}{|Z|}[R_{23} + \imath S_{23}], G_{33}^r = \frac{1}{|Z|}[P_{12} + \imath Q_{12}].$$

Where,

$P_{12} = b_1 b_2 - a^2 - \frac{1}{4}[g_7 g_8 - g_{13}]$, $P_{13} = b_1 b_3 - c^2 - \frac{1}{4}[g_7 g_9 - g_{14}]$

$P_{23} = b_2 b_3 - b^2 - \frac{1}{4}[g_8 g_9 - g_{15}]$,

$Q_{12} = \frac{1}{2}[b_1 g_8 + b_2 g_7 + 2a g_{10}]$, $Q_{13} = \frac{1}{2}[b_1 g_9 + b_3 g_7 + 2c g_{11}]$,

$Q_{23} = \frac{1}{2}[b_2 g_9 + b_3 g_8 + 2b g_{12}]$,

$R_{12} = ab_3 + bc + \frac{1}{4}[g_9 g_{10} - g_{11} g_{12}]$, $R_{13} = cb_2 + ab + \frac{1}{4}[g_8 g_{11} - g_{10} g_{12}]$,

$R_{23} = bb_1 + ac + \frac{1}{4}[g_7 g_{12} - g_{10} g_{11}]$,

$S_{12} = \frac{1}{2}\left[a g_9 - (b_3 g_{10} + c g_{12+} b g_{11)}\right]$,$S_{13} = \frac{1}{2}\left[c g_8 - (b_2 g_{11} + a g_{12+} b g_{10)}\right]$,

$S_{23} = \frac{1}{2}\left[b g_7 - (b_1 g_{12} + a g_{11+} c g_{10)}\right]$. (6)

In eqn. (6), various parameters are defined as,

$b_1 = \frac{b_{11} b_{12}}{b_{13}}$, $b_2 = \frac{b_{21} b_{22}}{b_{23}}$, $b_3 = \frac{b_{31} b_{32}}{b_{33}}$, (7)

with

$b_{11} = \omega - \epsilon_1$, $b_{12} = \omega - \epsilon_1 - U_1$, $b_{13} = \omega - \epsilon_1 - U_1(1 - < n_{1-\sigma} >)$,

$b_{21} = \omega - \epsilon_2$, $b_{22} = \omega - \epsilon_2 - U_2$, $b_{23} = \omega - \epsilon_2 - U_2(1 - < n_{2-\sigma} >)$,

$b_{31} = \omega - \epsilon_3$, $b_{32} = \omega - \epsilon_3 - U_3$, $b_{33} = \omega - \epsilon_3 - U_3(1 - < n_{3-\sigma} >)$. (8)

a, b and c in eqn. (6) denote interdot tunnel couplings t_{12}, t_{23} and t_{13} respectively and the parameters g's are as,

$g_7 = p + s$, $g_8 = q + t, g_9 = r + u$,

$g_{10} = g_{1+} g_4$, $g_{11} = g_{2+} g_5 g_{12} = g_{3+} g_6$,

$g_{13} = g_{10}^2$, $g_{14} = g_{11}^2$, $g_{15} = g_{12}^2$. (9)

also,

$p = \Gamma_{11}^L, q = \Gamma_{22,}^L \quad r = \Gamma_{33}^L$,

$s = \Gamma_{11}^R, t = \Gamma_{22,}^R \quad u = \Gamma_{33}^R$,

$$g_1 = \sqrt{pq}, g_2 = \sqrt{pr}, g_3 = \sqrt{qr},$$

$$g_4 = \sqrt{st}, g_5 = \sqrt{su}, g_6 = \sqrt{tu},$$

The denominator, Z, in eqn. (5) is expressed as, $Z = C_1^2 + C_2^2$. The expressions for C_1 and C_2 are given in Appendix B and $G^a = G^{r*}$.

6. Appendix B

The expressions for C_1 and C_2 in Appendix A are,

$$C_1 = C_{11} - C_{12} + \frac{1}{2}[C_{13} - C_{14}] + \frac{1}{4}[C_{15} - C_{16}],$$

$C_2 = \frac{1}{2}\left[C_{21} - C_{22} + 2(C_{23}+C_{24}) + \frac{1}{4}(C_{25}-C_{26})\right]$.

The various C_{ij} 's in above equation are given as,

$$C_{11} = b_1b_2b_3 - 2abc, C_{12} = gb_1 + hb_2 + fb_3,$$

$$C_{13} = ag_{11}g_{12} + bg_{10}g_{11} + cg_{10}g_{12},$$

$$C_{14} = ag_9g_{10} + bg_7g_{12} + cg_8g_{11}, C_{15} = b_1g_{15} + b_2g_{14} + b_3g_{13},$$

$$C_{16} = b_1g_8g_9 + b_2g_7g_9 + b_3g_7g_8,$$

$$C_{21} = b_1b_2g_9 + b_1b_3g_8 + b_2b_3g_7, C_{22} = fg_9 + gg_7 + hg_8,$$

$$C_{23} = bb_1g_{12} + cb_2g_{11} + ab_3g_{10},$$

$$C_{24} = bcg_{10} + abg_{11} + acg_{12}, C_{25} = g_7g_{15} + g_8g_{14} + g_9g_{13},$$

$$C_{26} = g_7g_8g_9 + 2g_{10}g_{11}g_{12}.$$

References

1. J. Gores, D. Goldhaber-Gordon, S. Heemeyer, M.A. Kastner, H. Shtrikman, D. Mahalu, U. Mirav, Phys. Rev. B 62 (2000) 2188.
2. A. W. Holleitner, C.R. Decker, H. Qin, K. Eberl, R. H. Blick, Phys. Rev. Lett. 87 (2001) 256802.
3. K. Kobayashi, H. Aikawa, S. Katsumoto, Y. Iye, Phys. Rev. Lett. 88 (2002) 256806.
4. W. G. van der Wiel, S. D. Franceschi, J. M. Elzerman, T. Fujisawa, S. Tarucha, L. P. Kouwenhoven, Rev. Mod. Phys. 75 (2003) 1.
5. U. Fano Phys. Rev. 124 (1961) 866.
6. M. L. L. de Guevara, P. A. Orellana, Phys. Rev. B 73 (2006) 205303.
7. H. Z. Lu, R. Lu, B. F. Zhu, Phys. Rev. B 71 (2005) 235320.
8. H. Z. Lu, R. Lu, B. F. Zhu, J. Phys.: Condens. Matter 18,(2006) 8961.
9. D. Sztenkiel, R. Swirkowicz, Physica E 40 (2008) 766.
10. J. C. Chen, A. M. Chang, M. R. Melloch, Phys. Rev. Lett. 92 (2004) 176801.
11. F. Chi, H. Zhao, Superlattices Microstruct. 47 (2010) 452.
12. D. Loss, D. DiVincenzo, Phys. Rev. A 57 (1998) 120.
13. G. Rajput, P. K. Ahluwalia, K. C. Sharma, EPL 94 (2011) 17003.
14. F. N. M. Froning, M. K. Rehmann, J. Ridderbos, M. Brauns, F. A. Zwanenburg, A. Li, F. R. Braakman, Applied Physics Letters 113 (2018) 073102.
15. B. Kratochwil, J. V. Koski , A. J. Landig, P. Scarlino, J. C. Abadillo-Uriel, C. Reichl, S. N. Coppersmith, W. Wegscheider, M. Friesen, A. Wallraff, T. Ihn, K. Ensslin, Physical Review Research 3 (2021) 013171.
16. A. Vidan, R. M. Westervelt, M. Stopa, M. Hanson, A. C. Gossard, Applied Physics

Letters 85 (2004) 16.

17. D. Krychowski, M. Antkiewicz, S. Lipi´nski, journal of magnetism and magnetic materials 541 (2022) 168564.
18. L. P. Keldysh, Sov. Phys. JETP 20 (1965) 1018.
19. P. W. Anderson, Phys. Rev., 124 (1961) 41.
20. G. Rajput, R. Kumar, Ajay, Superlattices and Microstructures 73 (2014) 193.

Figures

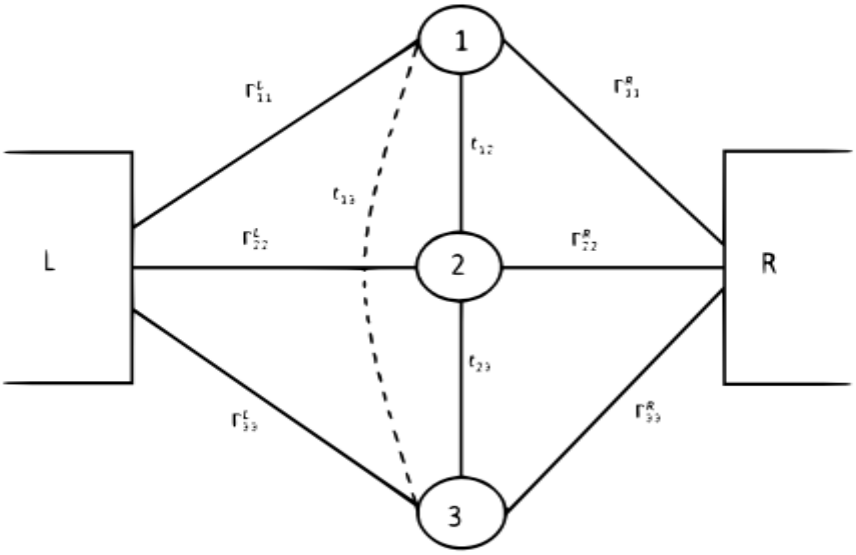

Figure 1: Schematic representation of generic TQD system with dot lead couplings. T-shape and Triangular shape configurations are obtained $\Gamma_{11}^{L} = \Gamma_{22}^{R} = \Gamma$and $\Gamma_{22}^{L} = \Gamma_{33}^{L} = \Gamma_{11}^{R} = \Gamma_{33}^{R} = 0$. The interdot tunnel couplings t_{12} and t_{23} and t_{13} are varied to get T-shape and triangular shape configurations.

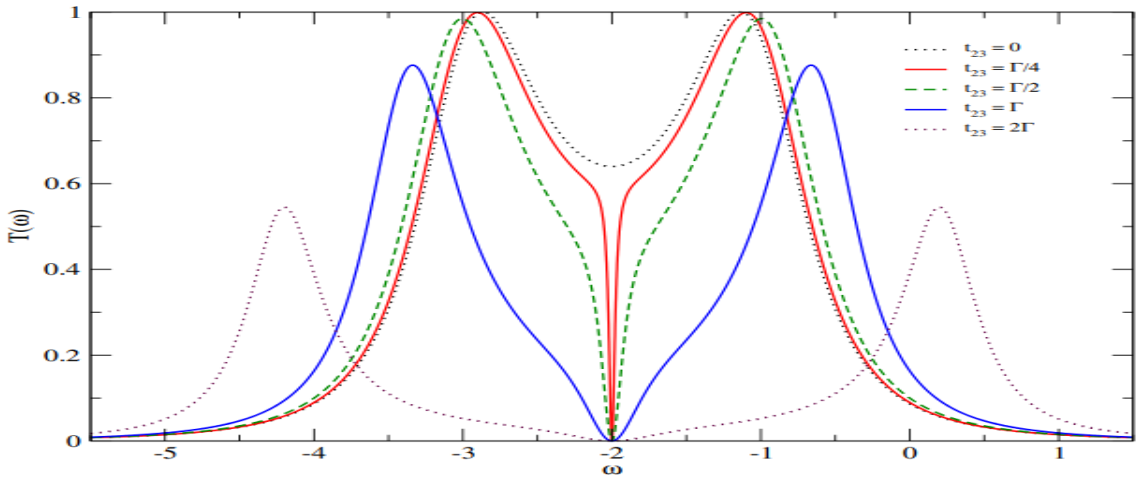

Figure 2: Displays T(ω) vs. ω curve for T-shape configuration of Double Quantum dot with interdot tunnel couplings, $t_{12} = \Gamma$, $t_{13} = 0$ and varying t_{23} in terms of Γ. Other parameters are $\epsilon_1 = \epsilon_2 = \epsilon_3 = \epsilon = -2\Gamma$ and various Γ's are defined in Fig.1.

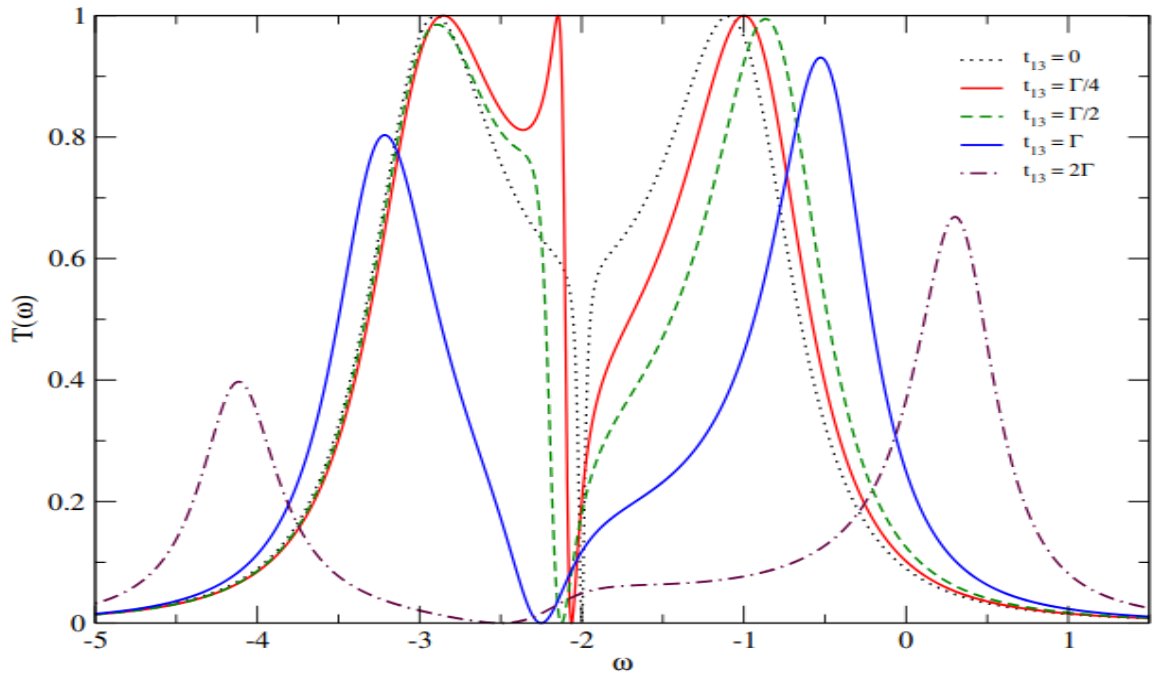

Figure 3: Displays T(ω) vs. ω curve for transitional change in configuration from T-shape to triangular shape of TQD system with interdot tunnel couplings, $t_{12} = \Gamma$, $t_{23} = \Gamma/4$ and varying t_{13}. Other parameters are same as in Fig. 2.